PFC/JA-85-41

Observations of Centrally Peaked Impurity Profiles in the Alcator-C Tokamak Following Pellet Injection

R. D. Petrasso, K. W. Wenzel, J. E. Hopf, D. J. Sigmar,
M. Greenwald, J. L. Terry and J. Parker[†]

December 1985

Plasma Fusion Center
Massachusetts Institute of Technology
Cambridge, Massachusetts, 02139 USA

[†] present address: Varian Associates, Beverly, MA 01915

This work was supported in part by the DOE, No. DE-AC02-78ET51013. Reproduction, translation, publication, use and disposal, in whole or in part, by or for the United States government is permitted.

Submitted to: Physical Review Letters, December 1985.

Abstract

Through use of x-ray arrays, highly peaked carbon (C) and molybdenum (Mo) profiles were observed to occur after pellet injection. Multi-ion neoclassical theory predicts equilibrium profiles close to these observations. Specifically, about 40 ms after pellet injection, C, a plateau impurity, was well fit by $(T_e/T_e(0))^{1.5Z_C}$ for $r \lesssim 6.5$ cm (Z_C=6). An internal disruption then occurred, which reduced on-axis impurities by a factor of 3 and terminated the neoclassical-like transport. Based on these observations, we posit that C, the dominant non-hydrogenic contributor to Z_{eff}, dramatically affects sawtooth dynamics by altering the central resistivity.

The transport of impurities, and the ensuing implications for current profiles and sawtooth dynamics, are crucial issues for tokamak physics and future reactor designs. In order to comprehensively study aspects of this problem, two x-ray arrays were designed with markedly different responses to Alcator's main light (C) and heavy (Mo) impurities (C and Mo are both limiter materials). Specifically, we studied their evolution following the injection of hydrogen pellets into deuterium plasmas.[1] This paper summarizes the observations and measurement technique, neoclassical predictions, and our conclusions. Discussion of improved energy confinement with pellet operation in Alcator has been reported elsewhere.[2]

Figure 1a depicts the x-ray spectral efficiences of the two arrays, A and B. Both are absolutely calibrated and conveniently cross-calibrated in-situ by operating with the same filter (A).[3,4] The arrays view the plasma from the same toroidal position, array A (B) from the side (bottom). For array B, with relevant Alcator conditions, only $\sim 2\%$ of the detected x rays are from Mo ions (mainly from Δn=2 transitions). This is because the filter response "cuts off" the dominant Δn=1 transitions that occur around 2.5 keV.[5]

The starting point for our analysis involves solving two equations for the C and Mo densities (n_C and n_M, respectively):

$$\frac{\epsilon^A}{n_e} - (P_H^A)n_H \simeq (P_C^A)n_C + (P_M^A)n_M \ ; \tag{1}$$

$$\frac{\epsilon^B}{n_e} - (P_H^B)n_H \simeq (P_C^B)n_C \ . \tag{2}$$

In these equations ϵ^A and ϵ^B are the absolute x-ray emissivities determined from Abel inversion; n_e is the electron density; $n_H = n_e - Z_C n_C - Z_M n_M$ [Z_C=6, $Z_M \approx 30$, and $Z_M n_M$ is negligible]; and the P_j^k's are spectral power functions for each species j, where j stands for either H, C, or Mo, and k = filter A or B. Figure 1b depicts array-B power functions for fully-stripped H and C ions (Gaunt corrected).[6] The power functions for Mo include collisional and dielectronic excitations (large contributions),[7] and bremsstrahlung and radiative recombination (small contributions). Appropriate weighted sums are taken over the central Mo ions, +28 thru +32.[8,7] Important to our analysis is the fact that the Mo power functions have a weak dependence on the precise weighting of these ions.

Time traces of several adjacent x-ray detectors are shown in Fig. 2 for a discharge with I_p=520 kA and B_t=9.7 T (major and minor radii of 64 cm and 16.5 cm). As the

pellet enters the plasma, the signals drop as $T_e(0)$ plummets from 1.6 keV to 0.6 keV. During the next 37 ms, T_e recovers and the C profile inside 7 cm gradually evolves from a "flattish" pre-pellet profile to a highly peaked one. The profile then abruptly "flattens" at the giant impurity disruption (henceforth abbreviated as G.I.D.), and thereafter carbon does not dramatically peak. Note that from pellet injection until the G.I.D., the carbon profile is modulated by sawteeth of increasing duration. Indeed, there are many discharges in which, following pellet injection, sawtoothing eventually stops. Figure 2c depicts array-A emissivities, determined through Abel inversion, at critical times in the discharge of Figs. 2a and 2b. It is worthwhile to stress that, contrary to "giant" internal disruptions attributed to large temperature fluctuations,[9] the G.I.D. is of a different nature (notice the small temperature drop in Fig. 3d). In fact, the temperature perturbation of the significantly smaller internal disruption following the G.I.D. (Fig. 2a), is virtually identical to that of the G.I.D.

Figures 3a and 3b show the experimentally determined C and Mo density profiles just prior to and after the G.I.D. The dashed curves are the asymptotic equilibrium profiles predicted on the basis of a rigorous multi-ion neoclassical theory.[10] In comparing experiment with theory, it is crucial to note that C is in the plateau regime (*ie.*, the C collision frequency is less than the transit frequency). Also, because of small Mo concentrations, diffusion of C is governed by its interaction with hydrogenic (H) ions. Thus the expression for the radial C flux is[10,11]

$$\Gamma_C \propto \left[\frac{n'_H}{n_H} - \frac{n'_C}{Z_C n_C} + \frac{1.5T'}{T}\right], \tag{3}$$

where T'/T is assumed to be the same for electrons and ions, and the prime indicates differentiation with respect to r. The exact source-free equilibrium solution to the continuity equation

$$\frac{\partial n_C}{\partial t} + \nabla \cdot \mathbf{\Gamma_C} = 0 \tag{4}$$

is, using Equation (3),

$$\left(\frac{n_C}{n_C(0)}\right) = \left(\frac{n_H}{n_H(0)}\right)^{Z_C} \left(\frac{T}{T(0)}\right)^{1.5Z_C}. \tag{5}$$

Equation (5) predicts that the temperature profile is responsible for peaking C since n_H is slightly hollow due to central ion deficit effects (Fig. 3e). Since Pfirsch-Schlüter (PS) theory is so often used to describe impurity transport, it is worthwhile to note that its

application would predict an equilibrium carbon profile that is actually *hollow*.[10,11] (The temperature term would become $(T(0)/T)^{0.5Z_C}$; the n_H term would remain unchanged.)

Because the experimental (pre-disruption) temperature profile is well represented by a Gaussian, Equation (3) can be accurately recast as

$$\Gamma_C = -Dn'_C - n_C V\left(\frac{r}{a}\right), \tag{6}$$

where a is the minor radius. D and V are not separately constant, though the ratio, D/V, is constant. From the experimental data at 257.5 ms, D/V is $0.33^{+0.18}_{-0.13}$ cm. This value is to be rigorously interpreted as an upper limit since array-B data indicate that some carbon peaking continues up to the onset of the large m=1 oscillation. (For example, see the center and outer signals in Fig. 2b.) However, close analysis of array-B signals reveals that ~75% of the signal change just prior to 257.5 ms is due to the increase in temperature, with only ~25% of the change due to additional carbon peaking.

The dashed curve in Fig. 3b depicts the asymptotic source-free equilibrium profile for Mo, predicted by the appropriate mixed-regime theory[10] (Mo in the PS regime, C and H in the plateau). The detailed application of this theory is lengthy, and is presented elsewhere.[12] It is concluded that Mo peaking is largely driven by the C profile. Thus, in analogy with Equation (5), and for our experimental conditions,

$$\left(\frac{n_M}{n_M(0)}\right) = \left(\frac{n_C}{n_C(0)}\right)^{\frac{Z_M}{Z_C}O_1}, \quad (0 \leq r \lesssim 4 \text{ cm}) \tag{7}$$

where O_1 is a correction factor of order 1 due to collision frequencies and mass ratios (temperature and hydrogen gradients are shown to be subdominant in shaping Mo profiles for $0 \leq r \lesssim 4$ cm).[12] Due to the larger error in the experimental molybdenum profile, the experimental width is determined to be between a factor of 1.3 and 3.0 that of the theory. In this context it is important to note that, on the basis of theory,[12,10] the asymptotic equilibrium profile for molybdenum should not be experimentally realized until ~20 ms after the carbon equilibrium profile is fully obtained.

Fitting and error analysis procedures are described next. Just prior to the G.I.D., impurity levels were observed to approach a minimum at about 6.5 cm, then rise outside this radius. Equations (1) and (2) were first used to estimate C and Mo profiles inside 6.5 cm. In turn these profiles were used to construct two Gaussians corresponding to n_C and

n_M, whose amplitudes and widths were varied until a good fit to the original data was achieved (see the *highly* peaked solid lines of Fig. 4). (The relative error in the x-ray data points is $\lesssim$ 5%; the absolute error is $\lesssim$ 10%.[3]) Errors in the e-folding widths (σ_C and σ_M) were then determined by varying n_e and T_e over their uncertainties: 15% in amplitude and 20% in width for n_e; 10% in amplitude and 20% in width for T_e. From this procedure, it was determined that $\sigma_C = 3.3^{+0.8}_{-0.7}$ cm, $\sigma_M = 3.5^{+0.5}_{-1.8}$ cm, and that the relative uncertainty in the on-axis ratio of C to Mo density is $\lesssim$2 (primarily due to the larger uncertainty in n_M). The experimental pre-disruption n_C and n_M profiles of Figs. 3a and 3b were determined through the use of the pre-disruption T_e and n_e profiles of Figs. 3c and 3d. Exactly the same profiles were used in evaluating the theoretical expressions, Equations (5) and (7) (depicted in Figs. 3a and 3b as the dashed curves).

The post-G.I.D. profiles were determined by finding acceptable fits to the change in the x-ray, interferometer (n_e), electron cyclotron (T_e), and visible bremsstrahlung signals. Starting with the pre-disruption profiles, n_e, T_e, n_C and n_M were "flattened" so as to conserve particles and energy to about 1%. Figure 3 depicts the post-disruption profiles,[13] and Fig. 4 the corresponding x-ray "reconstructions." The post-reconstructions do not fit the data as well as the pre-reconstructions, due in part to the greater uncertainty in post n_e and T_e profiles. In addition there is also a small – *but real* – up-down asymmetry that exists in the post x-ray data (Fig. 4a, data at $\pm$1.7 cm). Bearing in mind these considerations, the unambiguous effect of the G.I.D. is to reduce on-axis impurities by a factor of 3.

Finally we posit that central carbon, the dominant non-hydrogenic contributor to Z_{eff}, has directly measurable effects on the MHD dynamics associated with the sawtooth period. As carbon gradually peaks during the pellet reheat phase, the central Spitzer conductivity hollows (i of Fig. 3f), which leads to a "flattening" – possibly a hollowing – of the current profile. This will significantly reduce the m=1 tearing rate, conventionally associated with the sawtooth disruption,[14–16] since the growth rate scales as $q\prime(r_s)^2$. [$q\prime$ is the derivative of the safety factor, and r_s is the radius of the $q = 1$ singular surface.] The inhibition of the tearing mode should lengthen the sawtooth period, an effect observed during the reheat phase (Fig. 2a). If the current is sufficiently flat, the safety factor should be above 1 everywhere in the plasma. Indeed, this may account for the numerous discharges where sawteeth are completely suppressed following pellet injection. (Major

disruptions do not ensue for these cases.) In this situation, highly peaked impurity profiles persist. It is important to stress that this sawtooth suppression is not a result of a major change in central radiative power balance, since for the discharges discussed here, radiation plays an insignificant role in the central power balance. It is also directly relevant to this overall picture that the carbon profile is observed not to dramatically repeak after the G.I.D. [at which time the on-axis conductivity immediately rises (ii of Fig. 3f)], and that the sawtooth period becomes progressively shorter (by a factor of 2.5 approximately 15 ms after the G.I.D. of Fig. 2).

There are some striking parallels between these pellet observations and the gas-puffing experiments reported on Pulsator.[17] There it was observed that sawteeth were inhibited with a particular gas-puffing sequence (though the plasma subsequently disrupted). They interpreted these observations as due to a change in the central resistivity that occurred because of neoclassical impurity effects.

In summary, differently filtered x-ray arrays have been used to measure central carbon and molybdenum profiles, Alcator's dominant light and heavy impurities, following pellet injection. The width of the carbon profile is close to the neoclassical prediction of a source-free equilibrium state. The experimental molybdenum profile, which is more uncertain, is between a factor of 1.3 and 3.0 that of the asymptotic prediction; theory predicts, however, that the asymptotic molybdenum profile should not be experimentally realized until ~ 20 ms after the carbon equilibrium profile is fully obtained. We have no explanation why the injection of a pellet affects the impurity transport in the manner described, whereas for non-pellet discharges Alcator impurity transport is anomalous.[18] Nor is it clear why the giant impurity disruption (G.I.D.) should end this neoclassical-like behavior. In general, particle transport in tokamaks has been characterized as anomalous,[11] with several important exceptions.[11,17,19,20] Finally, we have presented direct evidence that the central peaking (flattening) of carbon lengthens (shortens) the sawtooth period – or stops the sawtooth altogether – through measured changes in the central Spitzer conductivity profile.

Acknowledgements

Special thanks to S. Wolfe, C. Gomez, M. Foord, E. Marmar, R. Granetz and J. Rice for interferometer, electron cyclotron, visible bremsstrahlung and x-ray data, and for helpful discussions. For assistance early in this project, we also thank F. Seguin and N. Loter. We appreciate the critical comments of I. Hutchinson and R. Benjamin. The excellent machine operation by the Alcator technical staff is gratefully acknowledged. This work has been supported in part by DOE contract DE-AC02-78ET51013.

References

1. J. L. Terry, *et al.*, Bull. of the Am. Phys. Soc. 28 (8) 1164 (1983).

2. M. Greenwald, *et al.*, Phys. Rev. Lett. 53 (4) 352 (1984).

3. R. D. Petrasso, *et al.*, Rev. Sci. Instrum. 51 (5) 585 (1980).

4. R. D. Petrasso, *et al.*, Phys. Rev. Lett. 49 (25) 1826 (1982).

5. Important to our analysis is the experimental observation by John Rice (MIT) that the intrinsic (*ie.* unfiltered) power ratio of $\Delta n=2$ to $\Delta n=1$ transitions is very small, approximately 1/12 at 1.6 keV. Private communication, 1985.

6. W. J. Karzas and R. Latter, Astrophys. J., Suppl. Ser. 6, 167 (1961).

7. E. Källne, J. Källne, and R. D. Cowan, Phys. Rev. A 27 (5) 2682 (1983).

8. C. Breton, C. DeMichelis, M. Finkenthal, and M. Mattioli, Association Euratom-C.E.A. #Eur-CEA-FC-948 (1978).

9. W. Pfeiffer, *et al.*, Nucl. Fusion 25 (6) 655 (1985).

10. S. P. Hirshman and D. J. Sigmar, Nucl. Fusion 21 (9) 1079 (1981); Eq. (6.129) for Mo, and Eqs. (7.43)-(7.48) for C in the plateau regime; Eq. (6.75) for C *if erroneously assumed* in the Pfirsch-Schlüter regime; references therein.

11. R. C. Isler, Nucl. Fusion 24 (12) 1599 (1984); Eq (43) for C in the plateau regime; approximately Eq. (42) for C *if erroneously assumed* in the Pfirsch-Schlüter regime; references therein.

12. D. J. Sigmar and K. W. Wenzel, manuscript in preparation.

13. Spectroscopic measurements of Mo^{+30} and Mo^{+31} density fluctuations were also obtained in response to the G.I.D. These fluctuations were much too large to be accounted for on the basis of recombination processes. Details of this work are in preparation (J. L. Terry and co-workers).

14. S. von Goeler, W. Stodiek, and N. Sauthoff, Phys. Rev. Lett. 33 (20) 1201 (1974).

15. B. V. Waddell, G. L. Jahns, J. D. Callen, H. R. Hicks, Nucl. Fusion 18 (5) 735 (1978).

16. G. Bateman, *MHD Instabilities*, MIT Press, p. 221 (1978); references therein.

17. W. Engelhardt, *et al.*, IAEA-CN-37/A-5, p. 123 (1978).

18. E. Marmar, J. Rice, J. Terry, and F. Seguin, Nucl. Fusion 22 (12) 1567 (1982).

19. G. L. Jahns, *et al.*, Nucl. Fusion 22 (8) 1049 (1982).

20. S. Sesnic, *et al.*; K. Ida, *et al.*, Bull. of Am. Phys. Soc. 30, 1438 (1985).

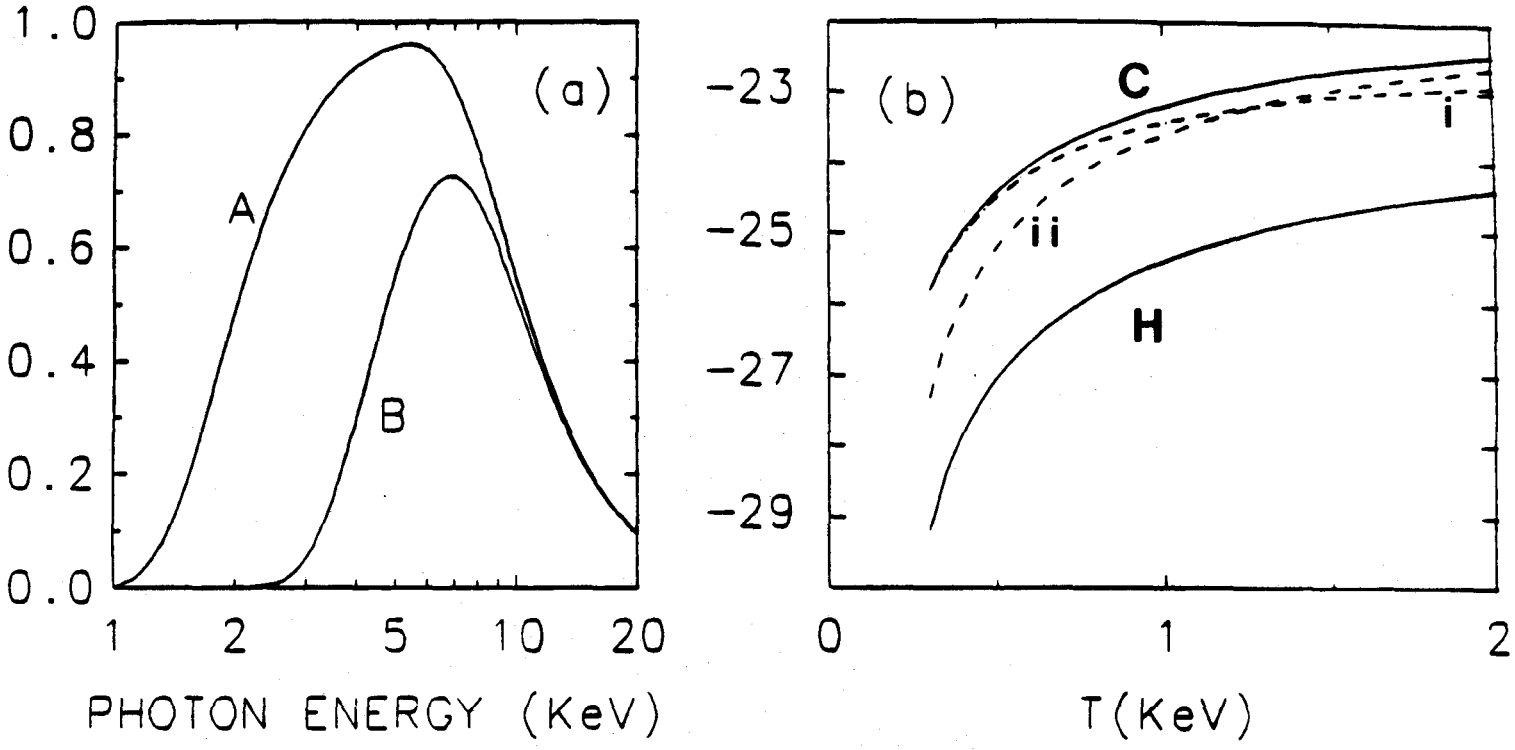

Fig. 1 (a) X-ray spectral efficiencies for arrays A and B. The low-energy response results from 10.0 mg/cm^2 Be for A; and from 10.0 mg/cm^2 Be plus 30.4 mg/cm^2 C for B. The high-energy response results from the finite detector thickness (23.3 mg/cm^2 Si). (b) Array-B power functions for the hydrogen (H) and carbon (C) x-ray continua. Recombination (i) and bremsstrahlung (ii) components of carbon are individually depicted, the former dominating for $T_e < 1.3$ keV [units of erg-cm^3/s; vertical scale in $\log_{10}$]. All calculations of the continua include appropriate Gaunt corrections.[6]

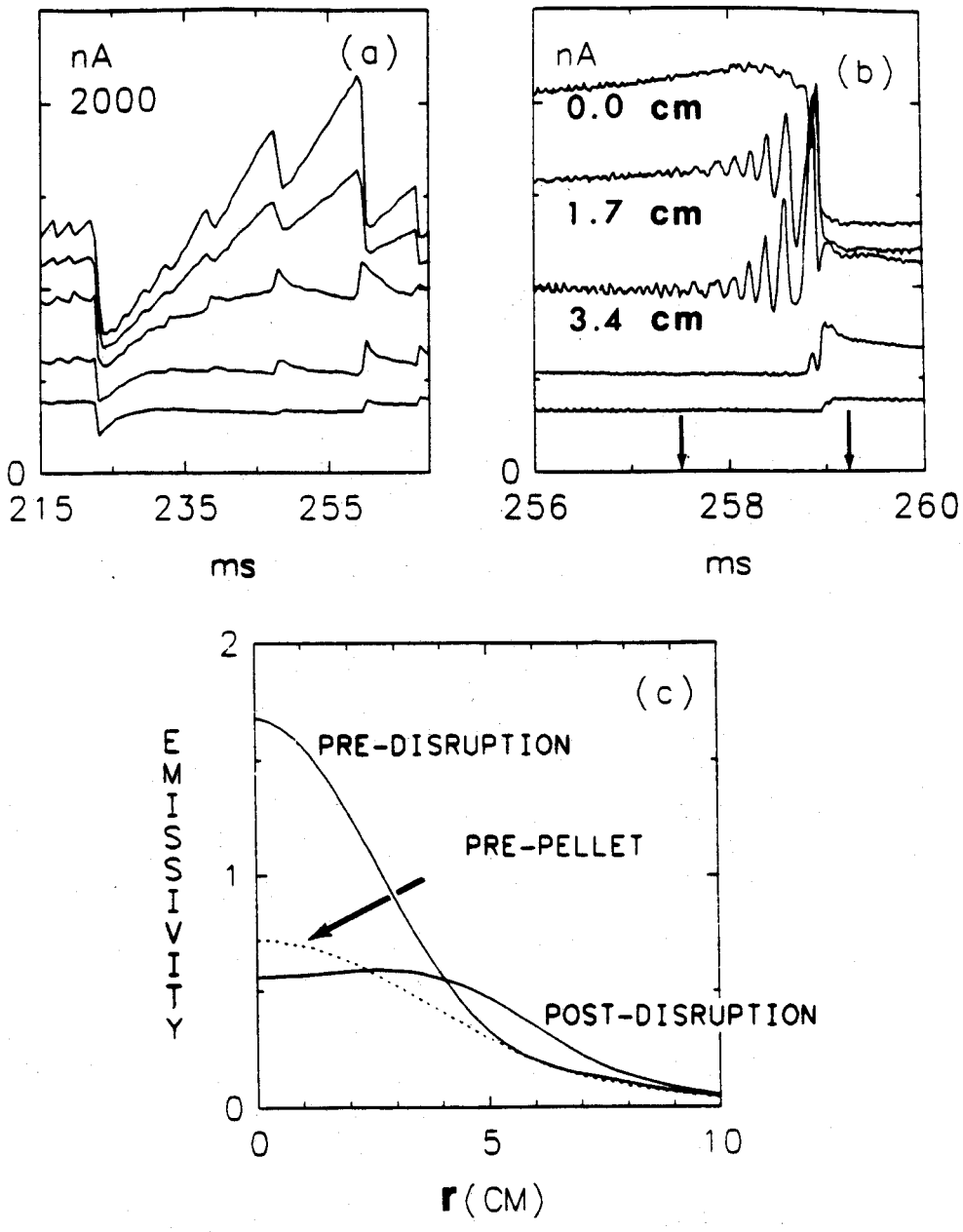

Fig. 2 (a) Several x-ray signals for adjacent array-A detectors viewing chords separated by 1.7 cm (shot # 25). The top signal corresponds to the center-viewing detector. The pellet enters the plasma at about 223 ms; the giant impurity disruption (G.I.D.) occurs at about 259 ms [units of nano-amps (nA)]. (b) Same as (a), but time-expanded about the G.I.D; the arrows indicate times of analysis for all subsequent figures. (c) Absolute array-A x-ray emissivities just before the pellet (dashed line), and just before (257.5 ms) and after (259.3 ms) the G.I.D. (solid lines) [units of 10^6 erg/(cm^3 s)].

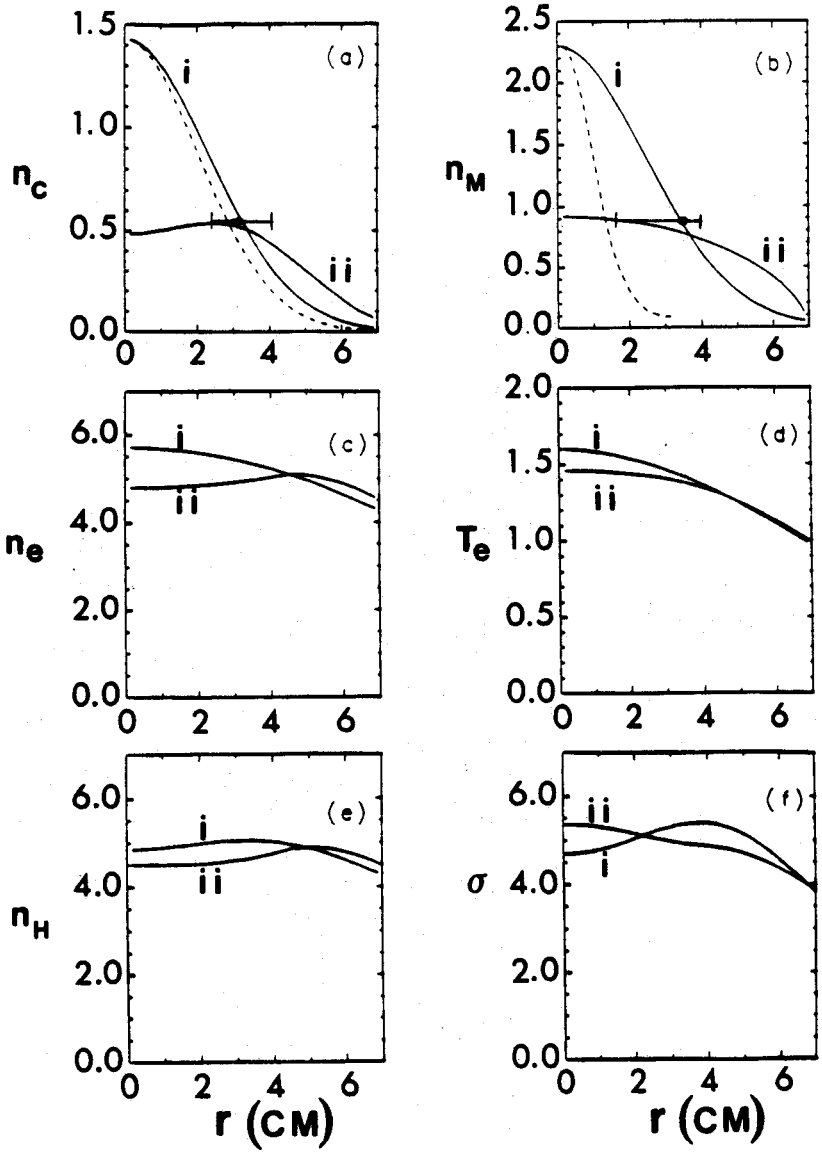

Fig. 3 (a) Experimental carbon density profiles just before (i) and just after (ii) the giant impurity disruption (G.I.D.), at the times indicated in Fig. 2b [units of 10^{13} cm^{-3}]. The dashed curve is the asymptotic equilibrium prediction. (b) Same as for (a), but for molybdenum [units of 10^{9} cm^{-3}]. (c) Corresponding n_e profiles [units of 10^{14} cm^{-3}]. (d) Corresponding T_e profiles [units of keV]. (e) Corresponding n_H profiles [units of 10^{14} cm^{-3}]. (f) Corresponding Spitzer conductivity profiles [units of 10^{5} (ohm-cm)$^{-1}$].

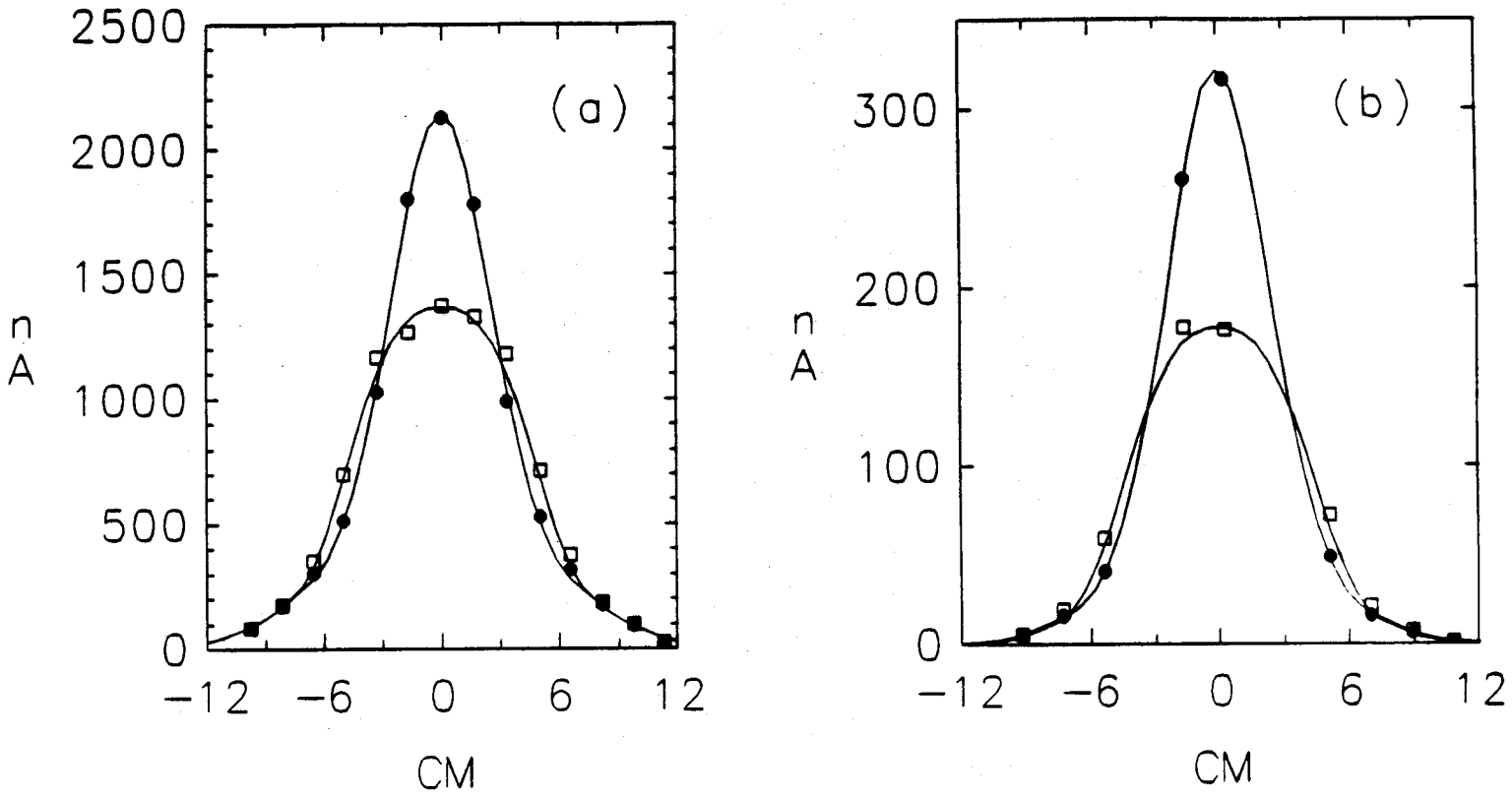

Fig. 4 (a) Array-A pre (•) and post (□) x-ray "brightness" data just before and just after the giant impurity disruption (G.I.D.) of Fig. 2. The lines are from "reconstructing" models of the x-emission, as described in the text [units of nano-amps (nA)]. (b) Same as (a), but for array B. [The relative error in all x-ray data points is $\lesssim$5%; the absolute error of the entire data set (A&B) is $\lesssim$10%. The noise level of each data point, ~0.5 nA,[3] is significantly smaller than the data-point symbols.]